

# A Computationally Efficient Maximum A Posteriori Sequence Estimation via Stein Variational Inference

Min-Won Seo and Solmaz S. Kia, *Senior Member, IEEE*

**Abstract**—State estimation in robotic systems presents significant challenges, particularly due to the prevalence of multimodal posterior distributions in real-world scenarios. One effective strategy for handling such complexity is to compute maximum a posteriori (MAP) sequences over a discretized or sampled state space, which enables a concise representation of the most likely state trajectory. However, this approach often incurs substantial computational costs, especially in high-dimensional settings. In this article, we propose a novel MAP sequence estimation method, **Stein-MAP-Seq**, which effectively addresses multimodality while substantially reducing computational and memory overhead. Our key contribution is a sequential variational inference framework that captures temporal dependencies in dynamical system models and integrates Stein variational gradient descent (SVGD) into a Viterbi-style dynamic programming algorithm, enabling computationally efficient MAP sequence estimation. **Stein-MAP-Seq** achieves a computational complexity of  $\mathcal{O}(M^2)$ , where  $M$  is the number of particles, in contrast to the  $\mathcal{O}(N^2)$  complexity of conventional MAP sequence estimators, with  $N \gg M$ . Furthermore, the method inherits SVGD's parallelism, enabling efficient computation for real-time deployment on GPU-equipped autonomous systems. We validate the proposed method in various multimodal scenarios, including those arising from nonlinear dynamics with ambiguous observations, unknown data associations, and temporary unobservability, demonstrating substantial improvements in estimation accuracy and robustness to multimodality over existing approaches.

**Index Terms**—Variational inference, maximum a posteriori (MAP) sequence estimation, Viterbi algorithm, dynamic programming, Stein variational gradient descent.

## I. INTRODUCTION

**S**TATE estimation in real-world robotic applications requires a reliable and efficient estimator. This paper focuses on the design of computationally efficient and accurate Maximum A Posteriori (MAP) *sequence* estimators for robotic systems. MAP sequence (MAP-Seq) estimation, due to its ability to handle complex, non-Gaussian distributions and leverage temporal dependencies in dynamical systems, is often sought after in estimation scenarios involving multimodal posterior distributions. These distributions frequently arise in challenging robotics tasks due to nonlinear system-environment interactions, ambiguous observations, uncertain data associations, and multimodal sensor fusion.

MAP-Seq estimators are an extension of MAP estimators, which seek the most probable state in a given distribution. MAP estimators are often preferred over Minimum Mean Square Error (MMSE) estimators for multimodal distributions, as MMSE estimators can produce estimates that lie between modes, potentially corresponding to low-probability regions

and leading to erroneous state estimates. In contrast, MAP estimation seeks the most probable state, effectively capturing one of the dominant modes in multimodal distributions. The MAP-Seq estimator extends this concept to find the most likely trajectory of states over a given time horizon, conditioned on the entire sequence of observations. This approach offers more robust estimates, particularly in scenarios with temporary unobservability or when the system's dynamics provide strong temporal constraints, by leveraging information across time to resolve ambiguities that may be present in point estimates. This framework has found applications across diverse domains, including image processing [1], natural language processing [2], and robotics for tasks such as high-level decision-making [3] and simultaneous localization and mapping (SLAM) or tracking [4], [5].

While MAP-Seq estimation offers significant advantages, computing the optimal trajectory can be computationally expensive, especially for complex, high-dimensional systems. One common approach uses smoothing techniques, such as iterated Extended Kalman Smoothing (iEKS) and factor graph optimization [6], which iteratively estimate the trajectory under Gaussian assumptions and local linearization. However, these methods often struggle with multimodal distributions, as they are prone to converging to *locally* optimal trajectories [5]. In contrast, approaches based on finite (discrete or sampled) state spaces, such as the Viterbi algorithm, compute the *globally* optimal trajectory via dynamic programming for MAP-Seq estimation [7], thereby avoiding local optima. This makes them particularly well-suited for estimation problems involving ambiguity, non-Gaussianity, or multimodality.

Despite this advantage, its computational complexity, which scales quadratically with the number of discrete states ( $\mathcal{O}(N^2)$  for  $N$  states), poses a significant bottleneck for real-time applications, especially when dealing with systems requiring fine-grained discretization of the state space for accurate representation. This limitation often restricts Viterbi algorithm's applicability to coarse-grid discretizations or necessitates the use of high-performance computing resources and substantial memory allocation in large-scale scenarios.

To overcome these computational hurdles, researchers have explored various strategies aimed at simplifying the representation of the state space [8], [9], [10], [11], [12], [13]. While such simplifications can lead to reduced computational demands, they often come at the cost of diminished estimation accuracy. Continuous-state-based Viterbi algorithms have been proposed [14], [15] to mitigate discretization errors, but these methods typically still grapple with significant computational complexity.

Particle Filter-based approaches for MAP-Seq estimation

Min-Won Seo, and Solmaz S. Kia are with the Department of Mechanical and Aerospace Engineering, University of California, Irvine, CA 92697, USA, {minwons, solmaz}@uci.edu

have also been investigated [16], [17], [18], [19], [20]. While these methods have shown promise in handling complex multimodal distributions, they still rely on sequential Monte Carlo methods, which require many particles and suffer from resampling overhead and random sampling variability.

In recent years, variational inference has emerged as a promising alternative for state estimation in complex systems. Variational methods aim to approximate intractable posterior distributions with simpler, tractable forms by framing inference as an optimization problem [21]. These techniques have gained attention in robotics and autonomous systems due to their ability to balance computational efficiency with the flexibility to capture complex, multimodal distributions [22], [23]. Notably, advances in variational inference have led to the development of methods that can handle non-Gaussian posteriors and temporal dependencies, making them particularly suitable for sequential estimation tasks [24], [25], [26]. The application of variational inference to state estimation problems has shown promise in various domains, including visual-inertial odometry [27], SLAM [28], and multi-target tracking [29].

*Statement of contribution:* This paper presents Stein-MAP-Seq, a novel particle-based approach for MAP-Seq estimation in dynamical systems that addresses the challenges of multimodal state estimation while maintaining computational efficiency. Our method leverages recent advances in variational inference, specifically Stein Variational Gradient Descent (SVGD) [30], a powerful non-parametric variational inference method. SVGD works by deterministically evolving a set of particles that serve as samples from the target distribution, minimizing the Kullback-Leibler divergence between the particle-based empirical distribution and the true posterior. Unlike traditional Monte Carlo methods that generate independent samples through stochastic processes, SVGD produces a deterministic set of interacting particles that collectively capture the structure of complex, potentially multimodal distributions.

The key innovation of Stein-MAP-Seq lies in leveraging these SVGD-generated particles as representative samples to transform the intractable continuous MAP optimization into an efficient discrete combinatorial problem. Stein-MAP-Seq embeds SVGD into a Viterbi-style dynamic programming algorithm within a sequential variational inference framework that explicitly models the temporal dependencies inherent in dynamical systems. This novel combination uniquely leverages SVGD's mode-seeking capability to deterministically generate a compact set of samples that concentrate around the modes of the posterior distribution, enabling efficient MAP sequence inference via dynamic programming over this discrete sample space using log probability-based scoring and backtracking. This approach effectively captures the complexity of multimodal posteriors while achieving a computational complexity of  $\mathcal{O}(M^2)$ , where  $M$  is the number of particles, a significant improvement over the  $\mathcal{O}(N^2)$  cost of the conventional MAP-Seq estimators with  $N \gg M$ . Furthermore, since the particle updates in SVGD can be computed independently for each sample, SVGD's inherent parallel nature makes Stein-MAP-Seq particularly well-suited for real-time deployment

on autonomous systems with parallel computing architectures [31], [32], [33], [34], [35].

Our approach fundamentally differs from traditional sampling-based methods by using SVGD's deterministic particle evolution to generate high-quality samples that are then used as discrete states in a Viterbi-style dynamic programming algorithm. We rigorously evaluate the proposed method on challenging scenarios, including nonlinear dynamics with ambiguous measurements, pose estimation under unknown data associations, and real-world range-only (wireless) localization under temporary unobservability, demonstrating substantial improvements in estimation accuracy and robustness to multimodality over state-of-the-art baselines.

The rest of this paper is organized as follows: Section II formally defines the problem and presents our assumptions. Section III provides a brief overview of SVGD. Section IV details our proposed Stein-MAP-Seq algorithm. Section V presents estimation results across diverse scenarios and compares them with existing methods. Finally, Section VI presents the conclusion.

## II. PROBLEM DEFINITION

Consider a discrete-time (fixed interval) dynamical system whose state transition probability is modeled as a Markov process (1a) and its observation likelihood function (1b) given by:

$$x_t \sim p(x_t|x_{t-1}), \quad (1a)$$

$$z_t \sim p(z_t|x_t), \quad (1b)$$

where  $x_t \in \mathbb{R}^{n_x}$  denotes the state of the system and  $z_t \in \mathbb{R}^{n_z}$  denotes the observation data at time  $t \in \mathbb{N}_{>0}$ . We assume that the prior distribution  $p(x_0)$  is constructed from available prior information. The dynamical model and observation data adhere to the following assumptions.

*Assumption 2.1:* (Smoothness and regularity of the dynamical model). Under the dynamical model (1),  $\log p(x_t|x_{t-1})$  and  $\log p(z_t|x_t)$  are continuously differentiable with respect to  $x_t$ , with Lipschitz continuous gradients.  $\square$

*Assumption 2.2:* (Assumptions on  $z_t$ ). The sensor observations at each time step,  $z_t$ , are independent and identically distributed (i.i.d.). Moreover, there are no conditional dependencies between observations from different sensors.  $\square$

Our objective in this paper is to compute the MAP sequence of states, denoted as  $x_{0:T}^{\text{MAP}}$ , for the dynamical system (1) from the sequence of observations from time 1 to the final time  $T$ , i.e.,  $z_{1:T} = \{z_1, \dots, z_T\}$ , given by

$$x_{0:T}^{\text{MAP}} = \underset{x_{0:T}}{\operatorname{argmax}} p(x_{0:T}|z_{1:T}). \quad (2)$$

Solving (2) is computationally intractable, particularly when  $p(x_{0:T}|z_{1:T})$  exhibits multimodality and/or lacks a closed-form expression, making exact analytical computation impossible. To address this challenge, we propose a *sequential variational inference* to obtain an approximate MAP sequence solution. The details of the proposed MAP formulation are presented in Section IV. Before presenting those details, the next section provides background on the Stein Variational Gradient Descent method, which is one of the key components of our approach.

**Algorithm 1:** Stein Variational Gradient Descent**Input:** The score function  $\nabla_x \log p(x)$ .**Goal:** A set of particles  $\{x_i\}_{i=1}^{N_s}$  that approximates  $p(x)$ .**Initialize** a set of particles  $\{x_i^{(0)}\}_{i=1}^{N_s}$ ; choose a positive definite kernel  $\kappa(x, x')$  and step-size  $\epsilon$ .**For** iteration  $l$  **do**

$$x_i^{(l+1)} \leftarrow x_i^{(l)} + \epsilon \hat{\phi}^*(x_i^{(l)}) \quad \forall i \in \{1, \dots, N_s\}$$

where  $\hat{\phi}^*(x_i^{(l)})$  is given in (4).

## III. A BRIEF OVERVIEW OF STEIN VARIATIONAL GRADIENT DESCENT METHOD

Variational inference (VI) approximates a target distribution  $p(x)$  using a simpler distribution  $q^*(x)$  found in a predefined set  $\mathcal{Q}$  by minimizing the Kullback–Leibler (KL) divergence [36], i.e.,

$$q^*(x) = \arg\min_{q \in \mathcal{Q}} \text{KL}[q(x) \parallel p(x)], \quad (3)$$

where the choice of the model space  $\mathcal{Q}$  is critical for balancing accuracy and computational efficiency; however, achieving this balance remains challenging.<sup>1</sup>

Stein Variational Gradient Descent (SVGD) offers a non-parametric approach by iteratively transporting a set of initial samples  $\{x_i^{(0)}\}_{i=1}^{N_s}$  towards  $p(x)$  using a perturbation function  $\phi(x)$ :

$$x_i^{(l+1)} = x_i^{(l)} + \epsilon \phi(x_i^{(l)}).$$

The optimal perturbation direction  $\phi^*(x) \in \mathcal{H}^d$  that minimizes the KL divergence at each step has a closed form derived from the Stein's identity<sup>2</sup>:

$$\phi^*(x) = \mathbb{E}_{x' \sim q(x)} [\kappa(x, x') \nabla_{x'} \log p(x') + \nabla_{x'} \kappa(x, x')],$$

where  $\kappa(x, x')$  is a positive definite kernel [30]. In practice, the perturbation direction is computed empirically using the samples  $\{x_i^{(l)}\}_{i=1}^{N_s}$ :

$$\hat{\phi}^*(x_i^{(l)}) = \frac{1}{N_s} \sum_{k=1}^{N_s} \left( \kappa(x_i^{(l)}, x_k^{(l)}) \nabla_{x_k^{(l)}} \log p(x_k^{(l)}) + \nabla_{x_k^{(l)}} \kappa(x_i^{(l)}, x_k^{(l)}) \right). \quad (4)$$

The update  $x_i^{(l+1)} = x_i^{(l)} + \epsilon \hat{\phi}^*(x_i^{(l)})$  iteratively pushes particles toward  $p(x)$ , enabling expectation approximations via the empirical mean. Algorithm 1 summarizes the Stein Variational Gradient Descent algorithm.

The samples generated by SVGD, denoted as  $\{x_i\}_{i=1}^{N_s}$ , serve a dual purpose in variational inference. First, they provide an empirical approximation of the optimal distribution  $q^*(x)$  in (3) as  $q^*(x) = \frac{1}{N_s} \sum_{i=1}^{N_s} \delta(x - x_i)$ . Second, and equally important, these particles are commonly interpreted as representative samples from the target distribution  $p(x)$  itself. Unlike traditional sampling methods such as MC or

MCMC, which generate independent samples through stochastic processes, SVGD produces a deterministic set of interacting particles that collectively capture the structure of complex, potentially multimodal distributions. This deterministic particle-based representation offers computational advantages for downstream tasks, including efficient parallel computation and natural handling of multimodal posterior structures. Consequently, SVGD has emerged as a powerful sampling tool for approximate inference in high-dimensional and multimodal scenarios where traditional sampling methods face significant challenges.

Conventional SVGD addresses stationary problems, whereas we extend it to sequential inference in a state estimation framework, as discussed in the next section.

## IV. STEIN MAXIMUM A POSTERIORI SEQUENCE ESTIMATION

In this section, we aim to develop a MAP sequence estimator for the dynamical system (1) by integrating a variational inference framework with dynamic programming. Computing the MAP trajectory  $x_{0:T}^{\text{MAP}}$  requires constructing an optimal distribution  $q^*(x_{0:T})$  whose support must be concentrated on the (unknown) global maxima of the true posterior  $p(x_{0:T}|z_{1:T})$ , and subsequently searching for these modes, making this task highly challenging. Formally, the problem can be stated as:

$$\begin{aligned} (q^*(x_{0:T}), x_{0:T}^{\text{MAP}}) = & \\ & \left( \arg \min_{q(x_{0:T})} \text{KL}[q(x_{0:T}) \parallel p(x_{0:T}|z_{1:T})], \arg \max_{x_{0:T}} q^*(x_{0:T}) \right). \end{aligned} \quad (5)$$

Solving these optimization problems exactly presents significant challenges. Particularly, when the dynamical system (1) is nonlinear, the resulting true posterior  $p(x_{0:T}|z_{1:T})$  becomes non-Gaussian and often multimodal, making its representation in closed-form impractical and exact analytical computation impossible. Moreover, the choice of  $q(x_{0:T})$  significantly impacts the performance of the estimation [16]. In the second optimization problem, finding the mode of  $q^*(x_{0:T})$  is not tractable, since  $q^*(x_{0:T})$  typically lives on a high-dimensional continuous support.

To address these limitations, we propose Stein-MAP-Seq, a MAP-sequence estimator for dynamical systems (1) that preserves temporal dependencies via a sequential variational-inference framework (Lemma 4.2). Stein-MAP-Seq integrates SVGD into a Viterbi-style dynamic programming framework, where SVGD's gradient flow provides a compact discrete state support, enabling efficient global MAP trajectory recovery via the Viterbi algorithm's forward recursion and backtracking.

Our approach addresses the intractability of the continuous optimization in (5) through a two-stage strategy: first, we use SVGD to generate particle-based approximations of the sequential posterior distributions, transforming the continuous state space into a finite discrete support; second, we apply dynamic programming over this discrete particle support to efficiently find the globally optimal MAP trajectory. This particle-based discretization fundamentally changes the nature

<sup>1</sup>KL divergence is defined as  $\text{KL}[q(x) \parallel p(x)] = \int q(x) \log \frac{q(x)}{p(x)} dx$ .

<sup>2</sup> $\phi^*(x)$  is chosen from the unit ball of a vector-valued RKHS,  $\mathcal{H}^d$ .

of the optimization from an intractable continuous search to an efficient discrete combinatorial problem.

The remainder of this section details the theoretical foundations and algorithmic steps of Stein-MAP-Seq, demonstrating how the two-stage combination of SVGD and Viterbi-style dynamic programming yields a robust and efficient MAP-sequence estimator.

### A. Sequential Variational Inference for Dynamical Systems

To make the complex optimization problems in (5) tractable and derive a computable solution for  $q^*(x_{0:T})$ , we begin by performing a series of strategic manipulations on the KL divergence objective

$$\text{minimize } \text{KL}[q(x_{0:T}) \parallel p(x_{0:T}|z_{1:T})]. \quad (6)$$

To facilitate a computable solution for VI optimization problems involving conditional posteriors based on measurements/data, it is common practice to reformulate the objective in terms of the Evidence Lower BOund (ELBO). In the case of (6), this relationship is given by:

$$\text{KL}[q(x_{0:T}) \parallel p(x_{0:T}|z_{1:T})] = -\mathcal{L}(x_{0:T}) + \log p(z_{1:T}), \quad (7)$$

where

$$\mathcal{L}(x_{0:T}) = \int q(x_{0:T}) \log \frac{p(x_{0:T}, z_{1:T})}{q(x_{0:T})} dx_{0:T} \quad (8)$$

is known as the ELBO; for a detailed derivation, see Lemma A.1 in Appendix A. The KL divergence in (7) is always nonnegative and equals zero if and only if  $q(x_{0:T}) = p(x_{0:T} | z_{1:T})$ . Moreover,  $\log p(z_{1:T})$  is constant with respect to  $x$  and does not affect the optimization. Therefore, minimizing the KL divergence, as shown on the left-hand side of (7), is equivalent to maximizing the ELBO  $\mathcal{L}(x_{0:T})$  defined in (8). Consequently, we reformulate the objective as the ELBO maximization problem, given by

$$q^*(x_{0:T}) = \arg\max_{q(x_{0:T})} \mathcal{L}(x_{0:T}), \quad (9)$$

where solving the optimization problem requires evaluating both the log joint probability  $\log p(x_{0:T}, z_{1:T})$  and the proposal distribution  $q(x_{0:T})$  within the ELBO.

To compute the log joint probability  $\log p(x_{0:T}, z_{1:T})$ , we factorize it based on the first-order Markov property of the dynamical system (1a) and Assumption 2.2 for observations  $z_{1:T}$ , yielding:

$$\log p(x_{0:T}, z_{1:T}) = \sum_{t=1}^T \log p(z_t|x_t) + \sum_{t=1}^T \log p(x_t|x_{t-1}) + \log p(x_0). \quad (10)$$

Using (10), the ELBO in (8) reads as

$$\begin{aligned} \mathcal{L}(x_{0:T}) = & \int q(x_{0:T}) \log p(x_0) dx_{0:T} \\ & + \int q(x_{0:T}) \sum_{t=1}^T \log p(x_t|x_{t-1}) dx_{0:T} \\ & + \int q(x_{0:T}) \sum_{t=1}^T \log p(z_t|x_t) dx_{0:T} \\ & - \int q(x_{0:T}) \log q(x_{0:T}) dx_{0:T}. \end{aligned} \quad (11)$$

The VI literature employs two broad techniques to specify the joint proposal distribution  $q(x_{0:T})$  in the ELBO: selecting a manageable parametric form [21], [28], [26], or employing the mean field approximation [7]. The first approach involves using a parameterized distribution, such as a Gaussian distribution. In the second approach, the joint proposal distribution is factorized into independent distributions for each time variable, i.e.,  $q(x_{0:T}) = \prod_{t=0}^T q(x_t)$ . These simplifications make the optimization process more tractable but may reduce approximation accuracy due to the inflexible distributional form and the loss of temporal dependencies.

Unlike existing techniques, in this study, we adopt a non-parametric method based on SVGD, which provides flexibility in approximating complex posterior structures. In addition, we impose a first-order Markov property on the proposal distribution to preserve temporal dependencies between adjacent states, an assumption that is naturally aligned with the sequential nature and underlying dynamics of the system, following the approach inspired by [37] as follows.

*Assumption 4.1:* (First-order Markov property on proposal distribution). The proposal distribution  $q(x_{0:T})$  in (9) is chosen such that

$$q(x_t|x_{t-1}) = q(x_t|x_{t-1}, x_{0:t-2}). \quad (12)$$

Under Assumption 4.1, we can show that the optimal solution of (9) admits the following factorized structure.

*Lemma 4.1:* (The form of optimal proposal distribution). Let Assumption 4.1 hold. Then, the optimal proposal distribution  $q(x_{0:T})$  in (9) is factorized as

$$q(x_{0:T}) = q(x_0) \prod_{t=1}^T q(x_t|x_{t-1}). \quad (13)$$

*Proof:* See Appendix B.  $\square$

According to Lemma 4.1, the proposal distribution  $q(x_{0:T})$  is factorized in (11). Consequently, the ELBO in (11) can be expressed as a summation of factorized KL divergence terms, each marginalized with respect to the previous optimal distribution, as stated in the following result.

*Lemma 4.2:* (The factorization of marginalized conditional KL divergence). Let Assumption 2.1, 2.2, and 4.1 hold. Given the optimal proposal distribution (13), the ELBO in (9) is factorized as

$$\begin{aligned} \mathcal{L}(x_{0:T}) = & -\text{KL}[q(x_0) \parallel p(x_0)] \\ & - \int \text{KL}[q(x_1|x_0) \parallel p(z_1, x_1|x_0)] q(x_0) dx_0 \\ & - \sum_{t=2}^T \int \text{KL}[q(x_t|x_{t-1}) \parallel p(z_t, x_t|x_{t-1})] q(x_{t-1}|x_{t-2}) dx_{t-1}, \end{aligned} \quad (14)$$

where  $p(z_t, x_t|x_{t-1}) = p(z_t|x_t)p(x_t|x_{t-1})$ .

*Proof:* See Appendix C.  $\square$

*1) SVGD-Based Sequential Approximation of Optimal Distributions:* The factorized ELBO structure in Lemma 4.2 reveals that the optimal proposal distribution can be computed sequentially by solving a series of marginalized conditional KL minimization problems. However, computing these optimal conditional distributions  $q^*(x_t|x_{t-1})$  analytically remains



intractable due to the complex, potentially multimodal nature of the target distributions  $p(z_t, x_t|x_{t-1})$ .

To address this computational challenge, we leverage SVGD's non-parametric approximation capabilities to sequentially construct particle-based representations of  $q^*(x_t|x_{t-1})$  for each time step. This approach transforms the continuous optimization problem into a manageable particle-based computation while preserving the temporal dependencies captured in the factorized ELBO.

The sequential particle generation procedure is as follows:

- 1) **Initialization** ( $t = 1$ ): Given the initial state  $x_0^{\text{true}}$  is known, we model its prior as a sharply concentrated Gaussian,  $p(x_0) = \mathcal{N}(x_0; x_0^{\text{true}}, \varepsilon \mathbf{I})$ ,  $\varepsilon \ll 1$ , then  $q^*(x_0) = p(x_0)$ <sup>3</sup>. For  $t = 1$ , given  $x_0^{\text{true}}$ , compute the distribution  $q^*(x_1|x_0) = \frac{1}{N_s} \sum_{i=1}^{N_s} \delta(x_1 - x_1^i)$ , where particles  $\{x_1^i\}_{i=1}^{N_s}$  are updated using SVGD with the following update direction:

$$\hat{\phi}^*(x_1^i) = \frac{1}{N_s} \sum_{k=1}^{N_s} \left[ \kappa(x_1^i, x_1^k) \nabla_{x_1^k} \log p(z_1, x_1^k | x_0^{\text{true}}) + \nabla_{x_1^k} \kappa(x_1^i, x_1^k) \right]. \quad (15)$$

- 2) **Sequential Particle Update** ( $t > 1$ ): For  $2 \leq t \leq T$ , given the set of particles  $\{x_{t-1}^i\}_{i=1}^{N_s}$  that empirically represent  $q(x_{t-1}|x_{t-2}) \approx \frac{1}{N_s} \sum_{i=1}^{N_s} \delta(x_{t-1} - x_{t-1}^i)$ , we aim to find a new set of particles  $\{x_t^i\}_{i=1}^{N_s}$ . These new particles should empirically estimate the optimal conditional distribution  $q^*(x_t|x_{t-1})$ , which is the solution to the following minimization problem:

$$q^*(x_t|x_{t-1}) = \arg \min_{q(x_t|x_{t-1})} \int \text{KL}[q(x_t|x_{t-1}) \| p(z_t, x_t|x_{t-1})] \times q(x_{t-1}|x_{t-2}) dx_{t-1} \quad (16)$$

Lemma 4.3 below presents the specific perturbation direction required to evolve the particles  $\{x_{t-1}^i\}_{i=1}^{N_s}$  to  $\{x_t^i\}_{i=1}^{N_s}$ , thereby empirically fitting  $q^*(x_t|x_{t-1})$  as defined in (16).

**Lemma 4.3:** (KL descent of marginalized conditional SVGD update). Let Assumption 2.1 and 4.1 hold, and define the marginalized KL divergence objective at time  $t$  as

$$\mathcal{J}_t(q) = \int \text{KL}[q(x_t|x_{t-1}) \| p(z_t, x_t|x_{t-1})] q(x_{t-1}|x_{t-2}) dx_{t-1}.$$

Given a set of particles  $\{x_{t-1}^j\}_{j=1}^{N_s}$  representing the distribution  $q(x_{t-1}|x_{t-2})$ , let the SVGD update direction be defined as

$$\hat{\phi}^*(x_t^i) = \frac{1}{N_s^2} \sum_{k=1}^{N_s} \sum_{j=1}^{N_s} \left[ \kappa(x_t^i, x_t^k) \nabla_{x_t^k} \log p(z_t, x_t^k | x_{t-1}^j) + \nabla_{x_t^k} \kappa(x_t^i, x_t^k) \right], \quad (17)$$

and apply the particle update:

$$x_t^i \leftarrow x_{t-1}^i + \varepsilon \hat{\phi}^*(x_{t-1}^i).$$

<sup>3</sup>This setup is essential for Theorem 4.1.

so that

$$q_\epsilon(x_t|x_{t-1}) = \frac{1}{N_s} \sum_{i=1}^{N_s} \delta(x_t - (x_{t-1}^i + \varepsilon \hat{\phi}^*(x_{t-1}^i))).$$

Then, under assumption of the boundedness of the kernel  $\kappa(\cdot, \cdot)$ , the marginalized KL objective satisfies

$$\left. \frac{d}{d\epsilon} \mathcal{J}_t(q_\epsilon) \right|_{\epsilon=0} < 0,$$

unless  $q(x_t|x_{t-1}) = p(z_t, x_t|x_{t-1})$  almost surely under  $q(x_{t-1}|x_{t-2})$ .

*Proof:* See Appendix D.  $\square$

This sequential SVGD procedure generates particle sets  $\{x_t^i\}_{i=1}^{N_s}$  for each time step  $t \in \{1, \dots, T\}$  that collectively provide a finite discrete approximation of the optimal proposal distribution  $q^*(x_{0:T})$ . The resulting particle-based representation transforms the intractable continuous MAP optimization problem into a discrete combinatorial problem that can be efficiently solved using dynamic programming, as detailed in the following subsection.

### B. Particle-Based Dynamic Programming for MAP Sequence Recovery

The sequential SVGD procedure described in the previous subsection generates particle sets  $\{x_t^i\}_{i=1}^{N_s}$  for each time step  $t \in \{1, \dots, T\}$  that empirically represent the optimal conditional distributions  $q^*(x_t|x_{t-1}) \approx \frac{1}{N_s} \sum_{i=1}^{N_s} \delta(x_t - x_t^i)$ . These particles serve as samples from the optimal distributions, providing a finite discrete approximation of the continuous state space at each time step. This particle-based representation transforms the continuous MAP optimization problem in (5) into a discrete combinatorial problem over finite particle sets.

Since  $\text{KL}[q^*(x_{0:T}) \| p(x_{0:T}|z_{1:T})] \rightarrow 0$  implies  $q^*(x_{0:T}) \rightarrow p(x_{0:T}|z_{1:T})$  in distribution [21], we have  $q^*(x_{0:T}) \propto p(x_{0:T}|z_{1:T})$  asymptotically. Consequently, given the particle sets  $\{x_t^i\}_{i=1}^{N_s}$  for all  $t \in \{1, \dots, T\}$ , an approximation to the MAP trajectory  $x_{0:T}^{\text{MAP}}$  in the second optimization in (5) is

$$\hat{x}_{0:T}^{\text{MAP}} = \arg \max_{x_{0:T} \in \{x_0^{\text{true}}\} \times \bigotimes_{k=1}^T \{x_k^i\}_{i=1}^{N_s}} p(x_{0:T}|z_{1:T}), \quad (18)$$

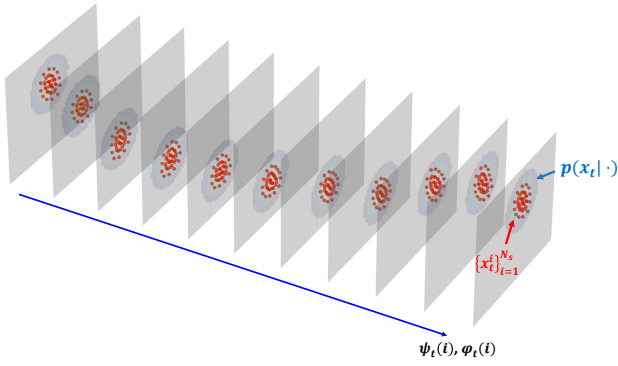
where  $\bigotimes_{k=1}^T$  is the Cartesian product over time steps from 1 to  $T$ . This implies that the trajectory  $x_{1:T}$  is selected from the product of particle sets across all time steps. As long as the support of  $q^*(x_{0:T})$  includes the support of  $p(x_{0:T}|z_{1:T})$ , the estimate  $\hat{x}_{0:T}^{\text{MAP}}$  converges asymptotically to  $x_{0:T}^{\text{MAP}}$  as  $N_s \rightarrow \infty$ .

Taking the logarithm of the posterior in (18) and exploiting the first-order Markov structure of the model (1a) and the conditional independence of observations (Assumption 2.2), we obtain, up to an additive constant:

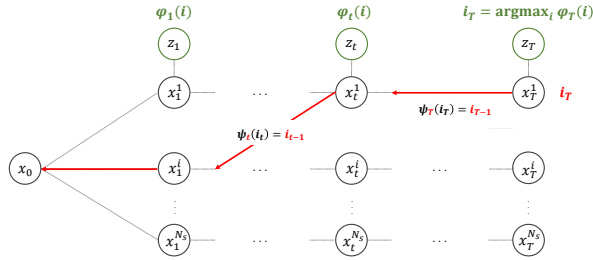
$$\log p(x_{0:T}|z_{1:T}) \propto \log p(x_0) + \sum_{t=1}^T \log p(x_t, z_t|x_{t-1}). \quad (19)$$

Therefore, the MAP trajectory approximation becomes:

$$\hat{x}_{0:T}^{\text{MAP}} = \arg \max_{x_{0:T} \in \{x_0^{\text{true}}\} \times \bigotimes_{k=1}^T \{x_k^i\}_{i=1}^{N_s}} \left[ \log p(x_0) + \sum_{t=1}^T \log p(z_t, x_t|x_{t-1}) \right]. \quad (20)$$



(a) Sequential particle update to obtain a finite discrete approximation of the state space.



(b) Backtracking the MAP sequence via the memorization table  $\psi(i)$ .

Fig. 1. Integration of SVGD-generated sequential particle sets with dynamic programming to yield globally optimal MAP trajectories.

**1) Viterbi-Style Dynamic Programming Algorithm:** The discrete optimization problem above can be efficiently solved using a Viterbi-style dynamic programming algorithm that leverages the temporal structure inherent in the factorized ELBO. The algorithm consists of two main phases: forward recursion for computing optimal accumulated scores, and backtracking for reconstructing the optimal sequence.

Finally,  $\hat{x}_{0:T}^{\text{MAP}} = (\hat{x}_0^{\text{MAP}}, \hat{x}_1^{\text{MAP}}, \dots, \hat{x}_T^{\text{MAP}})$  is efficiently found by dynamic programming over this discretized particle set. The steps are as follows:

**Forward Recursion.** For  $2 \leq t \leq T$  and for each particle  $x_t^i$  (where  $1 \leq i \leq N_s$ ), we compute  $\psi_t(i)$  (the index of the optimal preceding particle) and  $\varphi_t(i)$  (the maximum accumulated score to reach  $x_t^i$ ) as:

$$\psi_t(i) = \arg \max_{j \in \{1, \dots, N_s\}} \left\{ \log p(x_t^i | x_{t-1}^j) + \varphi_{t-1}(j) \right\}, \quad (21a)$$

$$\varphi_t(i) = \log p(z_t, x_t^i | x_{t-1}^{\psi_t(i)}) + \varphi_{t-1}(\psi_t(i)), \quad (21b)$$

where  $\varphi_1(i)$  is initialized based on  $\log p(z_1, x_1^i | x_0^{\text{true}})$ . This recursion ensures that  $\varphi_t(i)$  stores the maximum score for any path ending at particle  $x_t^i$ , by considering all possible preceding particles  $x_{t-1}^j$  and their optimal accumulated scores  $\varphi_{t-1}(\psi_t(i))$ .

**Backtracking the MAP Sequence.** After computing  $\varphi_T(i)$  for all  $i$ , the index of the optimal final particle is found as  $i_T = \arg \max_i \varphi_T(i)$ . The complete MAP sequence  $\hat{x}_{0:T}^{\text{MAP}}$  is then reconstructed by tracing back through the memorization table  $\psi_t(i)$  from  $t = T - 1$  down to 1:

$$\hat{x}_t^{\text{MAP}} = x_t^{i_t}, \quad \text{where } i_t = \psi_{t+1}(i_{t+1}),$$

with  $\hat{x}_0^{\text{MAP}} = x_0^{\text{true}}$ . This backtracking step ensures that the reconstructed path corresponds to the sequence of particles that yielded the maximum accumulated score, thereby identifying the MAP sequence estimator.

This two-stage approach offers a robust and computationally efficient solution for MAP sequence estimation in multimodal settings. First, SVGD flexibly captures complex posterior structures with a particle (support) set; then, particle-based dynamic programming decodes the optimal trajectory from these samples.

**2) Theoretical Guarantees and Computational Complexity:** The correctness of our particle-based dynamic programming approach is established through the connection between ELBO maximization and MAP trajectory recovery in the small- $\varepsilon$  regime, as formalized in the following theorem.

In summary, Stein-MAP-Seq computes the MAP sequence using a compact set of  $N_s$  particles at each time step  $t$ . The optimal sequence  $\hat{x}_{0:T}^{\text{MAP}}$  is obtained by backtracking through the memorization table  $\psi_t(i)$ , which is constructed from the accumulated scores  $\varphi_t(i)$  in Algorithm 2. In the small- $\varepsilon$  regime,  $\hat{x}_{0:T}^{\text{MAP}}$  coincides with the maximizer of the ELBO in Lemma 4.2, as stated in Theorem 4.1. For notational simplicity in Theorem 4.1, we let  $s$  denote an arbitrary candidate trajectory from  $\mathcal{S}$ , with  $s^*$  denoting the maximizer, i.e.,  $s^* = \hat{x}_{0:T}^{\text{MAP}}$ .

**Theorem 4.1:** (Equivalence of ELBO Maximization and the MAP Trajectory over Particle Sets in the Small- $\varepsilon$  Regime). Let Assumption 2.1 and 4.1 hold, and let  $\mathcal{S} \subseteq \{x_0^i\}_{i=1}^{N_s} \times \dots \times \{x_T^i\}_{i=1}^{N_s}$  denote the set of admissible trajectories over the particle sets. For  $s = (s_0, \dots, s_T) \in \mathcal{S}$ , define the trajectory score as

$$J(s) = \log p(s_0) + \sum_{t=1}^T \log p(s_t, z_t | s_{t-1}).$$

For  $\varepsilon > 0$ , define  $q_\varepsilon(x_0) = \mathcal{N}(x_0; s_0, \varepsilon \mathbf{I})$ ,  $q_\varepsilon(x_t | x_{t-1}) = \mathcal{N}(x_t; s_t, \varepsilon \mathbf{I})$  for all  $t = 1, \dots, T$ , and, from (14) in Lemma 4.2, let

$$\mathcal{L}_\varepsilon(s) := \mathcal{L}_\varepsilon(q_\varepsilon) + (T+1)H_\varepsilon,$$

where

$$\begin{aligned} \mathcal{L}_\varepsilon(q_\varepsilon) &= \mathbb{E}_{q_\varepsilon(x_0)} [\log p(x_0)] + \mathbb{E}_{q_\varepsilon(x_0)} \mathbb{E}_{q_\varepsilon(x_1 | x_0)} [\log p(z_1, x_1 | x_0)] \\ &\quad + \sum_{t=2}^T \mathbb{E}_{q_\varepsilon(x_{t-1} | x_{t-2})} \mathbb{E}_{q_\varepsilon(x_t | x_{t-1})} [\log p(z_t, x_t | x_{t-1})], \end{aligned}$$

and  $H_\varepsilon$  is the entropy of a Gaussian, which does not depend on  $s$  and is therefore constant. Then, for every  $s \in \mathcal{S}$ ,

$$\lim_{\varepsilon \rightarrow 0} \mathcal{L}_\varepsilon(s) = J(s).$$

Moreover,  $\mathcal{S}$  is finite, and suppose that there exists a unique  $s^* \in \arg \max_{s \in \mathcal{S}} J(s)$  with gap  $\delta := J(s^*) - \max_{s \neq s^*} J(s) > 0$ . Then there exists  $\varepsilon_0 > 0$  such that for all  $0 < \varepsilon < \varepsilon_0$ ,

$$\mathcal{L}_\varepsilon(s^*) > \mathcal{L}_\varepsilon(s) \quad \text{for all } s \neq s^*.$$

*Proof:* See Appendix E.  $\square$

Moreover, it substantially reduces both computational and memory requirements, as detailed below.

**Remark 4.1:** (Computational and Space Complexities). The Viterbi algorithm requires  $\mathcal{O}(N^2)$  computational complexity

**Algorithm 2: Stein-MAP-Seq**


---

**Input :** Transition probability  $p(x_t|x_{t-1})$ , initial state  $x_0^{\text{true}}$ , likelihood function  $p(z_t|x_t)$ , observations  $z_{1:T}$ , the number of particles  $N_s$ , the step size  $\epsilon$ .

```

// 1) Initialization ( $t = 1$ )
1 for  $i = 1, 2, \dots, N_s$  in parallel do
2    $x_1^i \leftarrow x_0^{\text{true}} + \epsilon \hat{\phi}^*(x_0^i)$ ,
3   where  $\hat{\phi}^*(x_0)$  from (15) given  $x_0^{\text{true}}$ 
4 end
5 for  $i \leftarrow 1$  to  $N_s$  do
6    $\varphi_1(i) = \log p(z_1, x_1^i | x_0^{\text{true}})$ 
7 end
// 2) Sequential Particle Update
8 for  $t = 2, \dots, T$  do
9   for  $i = 1, 2, \dots, N_s$  in parallel do
10     $x_t^i \leftarrow x_{t-1}^i + \epsilon \hat{\phi}^*(x_{t-1}^i)$ ,
11    where  $\hat{\phi}^*(x_t)$  from (17) given  $\{x_{t-1}^j\}_{j=1}^{N_s}$ 
12  end
// 3) Forward Recursion
13 for  $i \leftarrow 1$  to  $N_s$  do
14    $\psi_t(i) \leftarrow (21a)$ 
15    $\varphi_t(i) \leftarrow (21b)$ 
16 end
17 end
// 4) Backtracking
18  $i_T = \text{argmax}_i \varphi_T(i)$ 
19  $\hat{x}_T^{\text{MAP}} = x_T^{i_T}$ 
20 for  $t = T-1, \dots, 1$  do
21    $i_t = \psi_{t+1}(i_{t+1})$ 
22    $\hat{x}_t^{\text{MAP}} = x_t^{i_t}$ 
23 end
24  $\hat{x}_0^{\text{MAP}} = x_0^{\text{true}}$ 
25 return  $\hat{x}_{0:T}^{\text{MAP}} = \{\hat{x}_0^{\text{MAP}}, \hat{x}_1^{\text{MAP}}, \dots, \hat{x}_T^{\text{MAP}}\}$ 

```

---

and  $\mathcal{O}(NT)$  space complexity for the memorization table, where  $N$  is the number of discrete states. In general, achieving high accuracy necessitates a sufficiently large  $N$ . In contrast, Stein-MAP-Seq operates with a much smaller number of discrete states (particles), where  $N_s \ll N$ . Consequently, the computational complexity is reduced to  $\mathcal{O}(N_s^2)$  (with  $N_s^2 \ll N^2$ ) and the space complexity to  $\mathcal{O}(N_s T)$  (with  $N_s T \ll NT$ ). Furthermore, because the SVGD updates in (17) can be computed in parallel, Stein-MAP-Seq is well-suited for efficient execution on parallel computing devices (e.g., GPUs or multi-core CPUs). This contrasts with Monte Carlo sampling methods such as particle filters [38], where the resampling step introduces synchronization bottlenecks.  $\square$

In summary, Stein-MAP-Seq achieves efficient MAP sequence estimation through the synergistic combination of SVGD's flexible particle-based approximation and dynamic programming's optimal substructure exploitation. The method transforms the intractable continuous optimization into a manageable discrete problem while preserving the temporal dependencies essential for accurate sequential estimation.

## V. DEMONSTRATIONS

In this section, we rigorously evaluated the proposed method on challenging multimodal scenarios, including (A) nonlinear dynamics with *ambiguous* measurements, (B) pose estimation under *unknown* data associations, and (C) real-world range-only (wireless) localization under temporary *unobservability*.

We compared the performance of several state-estimation methods:

- **Extended Kalman Filter (EKF)** [39] and **Particle Filter (PF)** [40], both MMSE estimators, and **Extended Kalman Smoother (EKS)**, a MMSE sequence estimator;
- **Iterated EKF (iEKF)**, a (local) MAP estimator<sup>4</sup>, and **Iterated EKS (iEKS)**, a (local) MAP sequence estimator;
- **PF-based MAP estimate (PF-MAP)** [17] and **PF-based MAP-sequence estimate (PF-MAP-Seq)** [16];
- **Stein Particle Filter (SPF)** [34] and its MAP variant **SPF-MAP**, which applies the PF-MAP procedure to the SPF output.

All methods were implemented in Python and run on a laptop with an Intel Core i7-10510U CPU and 32GB of RAM. For the resampling step of the PF, we applied stratified sampling at every step. For the Stein series, we set  $\epsilon = 0.001$  and fixed the number of iterations to 1000 for all scenarios.

## A. 1D Nonlinear Dynamics with Ambiguous Measurement

In the first example, we consider a benchmark problem from [42], where the system model (1) is given by<sup>5</sup>

$$x_t = 0.9x_{t-1} + \frac{10x_{t-1}}{1 + x_{t-1}^2} + 8 \cos(1.2(t-1)) + v_{t-1}, \quad (22a)$$

$$z_t = 0.05x_t^2 + r_t, \quad (22b)$$

with  $v_{t-1} \sim \mathcal{N}(0, 5)$ ,  $r_t \sim \mathcal{N}(0, 10)$  and  $x_0 \sim \mathcal{N}(0, 5)$ . The significance of this example is that the term  $x_t^2$  in (22b) introduces a sign ambiguity, e.g.,  $x_t = +a$  and  $x_t = -a$  yield the same measurement, resulting in a bimodal posterior (see Fig. 2, top)

To evaluate the state estimation methods, we generated 50 independent trajectories of 100 time steps each. For each estimator, we computed the root-mean-square error (RMSE) of the state estimates, averaged over all Monte Carlo runs. The results in Fig. 2, bottom, Fig. 3, and Table I demonstrated that Stein-MAP-Seq significantly outperformed several state estimation methods, indicating that Stein-MAP-Seq is robust to bimodal posterior distributions. This performance advantage can be attributed to the mode-seeking behavior of SVGD, even with a small number of particles, and the use of Viterbi-style dynamic programming to identify the globally optimal trajectory over the sampled space.

The methods, such as EKF, EKS, iEKF-3, and iEKS-3, rely on Gaussian (unimodal) assumptions and local linearization in filtering and smoothing, making them prone to converge to locally optimal trajectories. In this setup, iEKF-3 and iEKS-3

<sup>4</sup>The iterative procedure can be interpreted as the Gauss-Newton method for finding the MAP estimate at the correction step [41].

<sup>5</sup>The models correspond to the form  $x_t \sim p(x_t|x_{t-1}) = \mathcal{N}(f(x_{t-1}), v_{t-1})$  and  $z_t \sim p(z_t|x_t) = \mathcal{N}(h(x_t), r_t)$ .

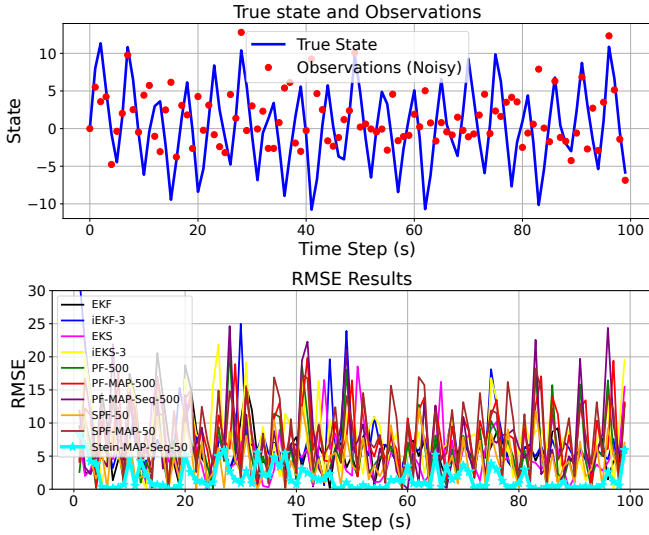


Fig. 2. **(Top)** True state and noisy observations (red dots) with sign ambiguity, resulting in a bimodal posterior distribution. **(Bottom)** One Monte Carlo simulation result. The simulation showed that Stein-MAP-Seq (cyan solid line with markers) significantly outperformed several state estimation methods, demonstrating robustness to bimodal posterior distributions.

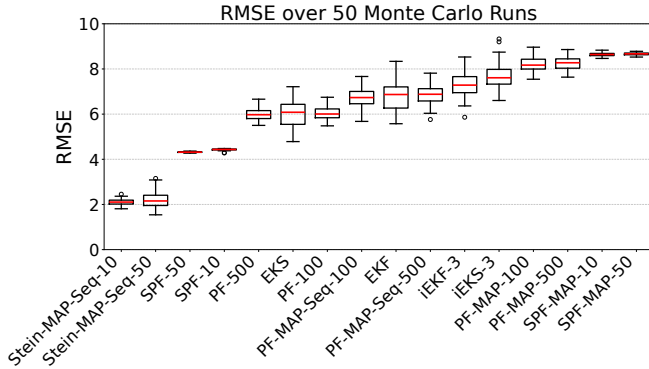


Fig. 3. Results from 50 Monte Carlo simulations over 100 steps under nonlinear dynamics with ambiguous measurements. In sampling-based methods, the number following each method name indicates the particle count; in Gaussian-based methods, it indicates the number of iterations.

were initialized with EKF and iEKF-3 estimates, respectively, and refined the trajectory through iterative forward-backward local linearization. The number following the method name denotes the iteration number. iEKF-3 and iEKS-3 showed worse performance than EKF and EKS because their initial trajectories were suboptimal, and in the presence of a bimodal posterior, local optimization reinforced incorrect estimates.

For PF-MAP-Seq, even with a large number of particles (100 or 500) relying on random sampling, its mode-seeking capability was weaker than that of Stein-MAP-Seq, which used significantly fewer particles (10 or 50). In the case of PF-MAP and SPF-MAP, the estimators converged to an incorrect mode due to sign ambiguity in the observations and the lack of temporal dependency modeling, operating on points rather than entire trajectories. This led to the worst estimation performance, even worse than MMSE estimators such as EKF, PF, and SPF.

TABLE I  
ROBUSTNESS EVALUATION FOR SCENARIO (A), AVERAGED RMSE

EKF	EKS	$N_s$	PF	PF-MAP	PF-MAP-Seq
6.7678	<b>6.0377</b>	1e2	6.0441	8.1799	6.7130
		5e2	6.0071	8.2770	6.8770
		1e3	<b>5.9816</b>	8.2658	6.9237
iEKF-3	iEKS-3	$N_s$	SPF	SPF-MAP	Stein-MAP-Seq
7.3307	7.6991	1e1	4.4294	8.6393	<b>2.1058</b>
		5e1	4.3164	8.6605	2.1881
		1e2	4.3127	8.6848	2.3284

Among the Stein variants, SPF is an MMSE estimator, while SPF-MAP provides a point-wise MAP estimate. Both are outperformed by Stein-MAP-Seq, which explicitly models temporal dependencies across the trajectory. Interestingly, for Stein-MAP-Seq, using 10 particles results in better performance than using 50 or 100 particles. In SVGD, each particle update is influenced by all other particles through the kernel term (the second term in (17)), and excessive repulsion can push particles into low-density regions to maintain diversity, which can negatively affect mode-seeking behavior.

#### B. Pose Estimation under Unknown Data Association

In the second example, we consider pose estimation on SE(2) under unknown data association. The discrete-time pose is updated by

$$\begin{bmatrix} x_t \\ y_t \\ \theta_t \end{bmatrix} = \begin{bmatrix} x_{t-1} + v_t \Delta t \cos \theta_t \\ y_{t-1} + v_t \Delta t \sin \theta_t \\ \theta_{t-1} + \omega_t \Delta t \end{bmatrix}, \quad (23)$$

with the pose process noise  $\mathcal{N}(\mathbf{0}, \mathbf{Q}_{t-1})$  where  $\mathbf{Q}_{t-1} = \text{diag}[(\alpha_x \Delta t)^2, (\alpha_y \Delta t)^2, (\alpha_\theta \Delta t)^2]$ . The state vector is  $\mathbf{x}_t = [x_t, y_t, \theta_t]^\top$  ( $m, m, \text{rad}$ ) with control inputs  $[v_t, \omega_t]^\top$  ( $m/s, \text{rad/s}$ ), and  $\Delta t$  denotes the sampling period. Here,  $\alpha_x$  and  $\alpha_y$  quantify translational noise per unit time along the body-fixed  $x$  and  $y$  axes, and  $\alpha_\theta$  quantifies rotational noise per unit time. In our simulation, we use  $\alpha_x = \alpha_y = 0.05$ ,  $\alpha_\theta = 0.035$ ,  $\Delta t = 0.1$ , and initialize the covariance as  $\Sigma_0 = \text{diag}[0.2^2, 0.2^2, 0.035^2]$ .

The range and bearing measurements to landmark  $l$  are given by:

$$z_{t,l}^r = \|\Gamma_l - P_t\|_2 + r_{t,l}^r, \quad (24a)$$

$$z_{t,l}^b = \text{atan2}(y_t - \Gamma_{l,y}, x_t - \Gamma_{l,x}) + r_{t,l}^b, \quad (24b)$$

where  $z_{t,l}^r \in \mathbb{R}_{\geq 0}$  ( $m$ ),  $z_{t,l}^b \in [-\pi, \pi]$  ( $\text{rad}$ ),  $\Gamma_l = [\Gamma_{l,x}, \Gamma_{l,y}]^\top \in \mathbb{R}^2$  is the  $l$ -th anchor position, and  $P_t = [x_t, y_t]^\top \in \mathbb{R}^2$  is the robot's position at time  $t$ . Here,  $\|\cdot\|_2$  denotes the Euclidean norm, and the measurement noises are  $r_{t,l}^r \sim \mathcal{N}(0, 1^2)$  and  $r_{t,l}^b \sim \mathcal{N}(0, 0.17^2)$ .

In this scenario, the robot receives observations from four landmarks with unknown data associations. For a given measurement  $\mathbf{z}_t = [z_t^r, z_t^b]^\top$ , the identity of the generating landmark  $l$  is unknown. To address this, we marginalize over  $l$ , yielding the association-marginalized (data-association-free) likelihood below:

$$p(\mathbf{z}_t | \mathbf{x}_t) = \sum_{l=1}^4 p(\mathbf{z}_t | \mathbf{x}_t, l) p(l), \quad (25)$$



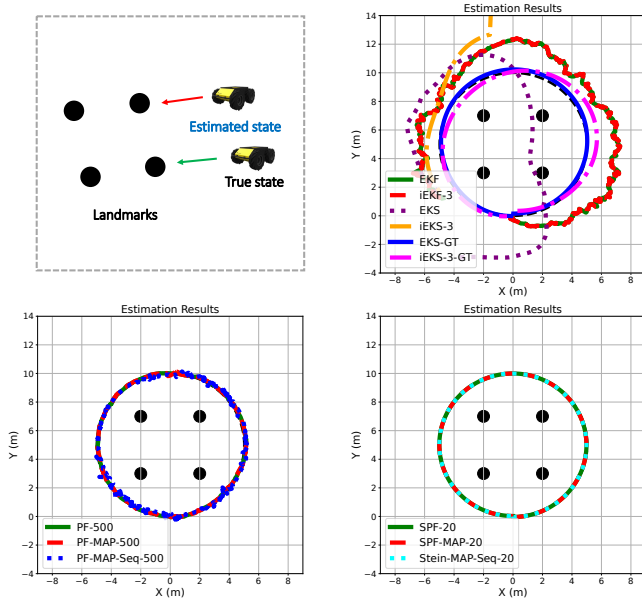


Fig. 4. One Monte Carlo simulation: a robot receives observations from 4 landmarks with unknown data associations, producing a multi-peak posterior. Stein-based estimation outperformed Gaussian-based and PF-based estimation.

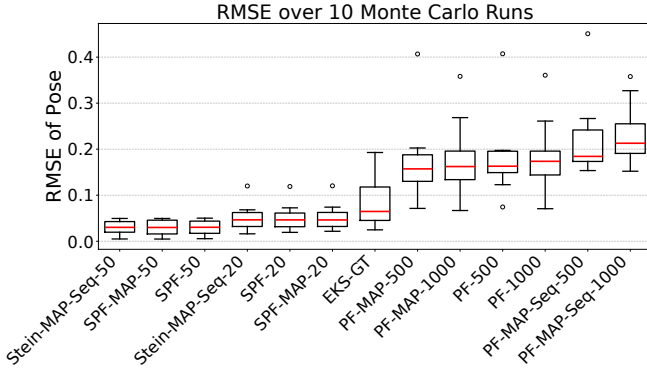


Fig. 5. Results from 10 Monte Carlo simulations over 630 steps for pose estimation under unknown data association. Methods are ordered from left to right by increasing RMSE.

where  $p(l) = \frac{1}{4}$ . This results in an equally weighted mixture of the four single-landmark likelihoods, producing a multimodal posterior distribution with multiple peaks (similar to a Gaussian mixture model).

To evaluate the state estimation methods, we generated 10 independent trajectories of 630 time steps each. For each estimator, we computed the RMSE of the state estimates, averaged over all Monte Carlo runs. The results in Fig. 4, Fig. 5, and Table II demonstrated that Stein-MAP-Seq significantly outperformed several state estimation methods, indicating that Stein-MAP-Seq is robust to multimodal posterior distributions.

Gaussian-based methods, such as EKF, EKS, iEKF-3, and iEKS-3, were not robust to multi-peak posterior distributions. To assess the effect of initialization in iterative methods, we also implemented EKS-GT and iEKS-3-GT, both initialized at the ground truth. Monte Carlo results for EKS-GT were

TABLE II  
ROBUSTNESS EVALUATION FOR SCENARIO (B), AVERAGED POSE RMSE

EKF	EKS	EKS-GT	$N_s$	PF	PF-MAP	PF-MAP-Seq
2.1028	2.4934	<b>0.0832</b>	5e2	0.1818	<b>0.1745</b>	0.2240
			1e3	0.1845	0.1787	0.2313
			2e3	0.1872	0.1812	0.2442
iEKF-3	iEKS-3	iEKS-3-GT	$N_s$	SPF	SPF-MAP	Stein-MAP-Seq
2.1070	> 100	> 100	2e1	0.0514	0.0522	0.0510
			4e1	0.0382	0.0375	0.0394
			5e1	0.0299	0.0298	<b>0.0293</b>

generally close to the ground truth (see Fig. 4, 1st quadrant). In contrast, iEKS-3-GT produced worse estimates than EKS-GT, with performance degrading further as the number of iterations increased. This degradation occurs because each re-linearization step perturbs the linearization point due to process and measurement noise, potentially causing the estimate to drift away from the true state in nonlinear and multimodal settings.

Among PF-based methods, PF-MAP with 500 particles achieved the best performance (Table II and Fig. 5). PF-MAP outperformed PF, an MMSE estimator, across all tested particle counts. In contrast, PF-MAP-Seq exhibited mode switching, resulting in a zig-zag trajectory and the poorest estimation performance (see Fig. 4, 3rd quadrant). We also observed that, even as the number of particles increased, the estimation performance of PF-based methods tended to degrade. This indicates that more particles do not necessarily provide a better representation of the posterior. Even with importance sampling, randomly drawn particles often populate intermediate-probability regions (neither high nor low), which reduces their concentration around the true mode and consequently degrades estimation accuracy.

Stein-series methods outperformed both Gaussian-based and PF-based methods. In particular, Stein-MAP-Seq with 50 particles achieved the best overall performance (Table II). For SPF, SPF-MAP, and Stein-MAP-Seq, estimation performance improved with increasing particle count up to 50.

### C. Range-only Localization under Temporary Unobservability

In the last example, we consider a range-only localization task [43], [44]. In our experiment, a target equipped with a DWM1000 Ultra-wideband (UWB) transceiver (tag) traversed along an *arbitrary trajectory* in an  $8\text{ m} \times 8\text{ m}$  indoor environment with 3 UWB anchors. Here, UWB provides range measurements at 10 Hz and can also communicate their IDs, eliminating the need for data association considerations. There were no obstacles between the anchors and the tag to mitigate the biased range measurements. For a precise reference trajectory comparison, we employed the OptiTrack optical motion capture system with 12 infrared cameras to achieve high precision localization with an accuracy of  $10^{-4}\text{ m}$ , and a sampling rate of 120 Hz.

We localize a target that is not equipped with any proprioceptive sensor, such as an IMU or encoders. Consequently, we adopt a zero-velocity motion model, given by

$$\mathbf{x}_t = \mathbf{x}_{t-1} + \mathbf{v}_{t-1}, \quad (26)$$

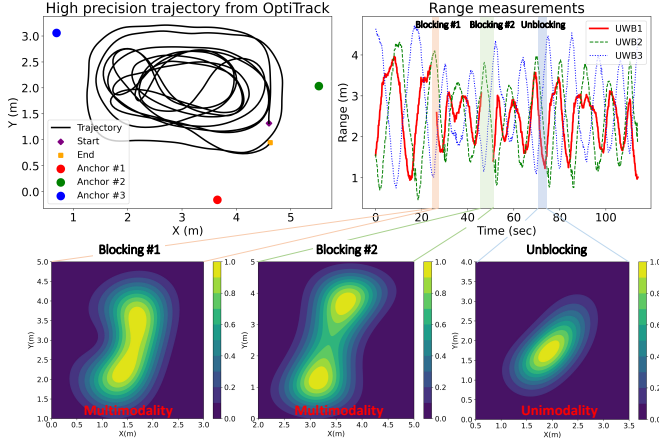


Fig. 6. A target traversed an arbitrary trajectory captured by the OptiTrack system at 120Hz, while a UWB sensor provided range measurements at 10Hz. During the 114.5 s experiment, one tag and three anchors remained fully connected except during temporary blocking periods (i.e., intervals of unobservability). Anchor #1 was blocked multiple times, leaving connections only to anchors #2 and #3, which induced multimodality in the measurement likelihood. The contour plots of the likelihood function during Blocking #1 and Blocking #2 show multimodal distributions, whereas the Unblocking period exhibits a unimodal distribution.

where the process noise is modeled as  $\mathbf{v}_{t-1} \sim \mathcal{N}(\mathbf{0}, \mathbf{Q}_{t-1})$ , with  $\mathbf{Q}_{t-1} = \text{diag}[(\alpha_x \Delta t)^2, (\alpha_y \Delta t)^2]$ . The state vector  $\mathbf{x}_t = [x_t, y_t] \in \mathbb{R}^2 (m)$  represents the 2D position at time  $t$ . We use line-of-sight (LoS) range measurements of the form:

$$z_{t,l} = \|\Gamma_l - \mathbf{x}_t\|_2 + r_{t,l}, \quad (27)$$

where  $z_{t,l} \in \mathbb{R}_{\geq 0} (m)$  is the LoS range to the  $l$ -th anchor at time  $t$ ,  $\Gamma_l = [\Gamma_{l,x}, \Gamma_{l,y}]^\top \in \mathbb{R}^2$  denotes the anchor position,  $\|\cdot\|_2$  denotes the Euclidean norm, and the measurement noise is  $r_{t,l} \sim \mathcal{N}(0, \sigma_z^2)$ . The likelihood function over all range measurements is expressed as:

$$p(\mathbf{z}_t | \mathbf{x}_t) = \prod_{\forall l} p(z_{t,l} | \mathbf{x}_t), \quad (28)$$

where the product arises from the Assumption 2.2. In this experiment, we set  $\alpha_x = \alpha_y = 1.0$ ,  $\Delta t = 0.1$ , and  $\sigma_z = 0.5$  to model measurement noise and compensate for minor range bias.

In this scenario, some anchors may be blocked by dynamic or static obstacles, leading to a multimodal distribution due to the underdetermined nature of distance measurements. In the experiment, we dropped measurements from anchor #1 at specific time instances to simulate real-world (underdetermined) scenarios for robustness analysis against a *symmetric* multimodality, see Fig 6.

We evaluated the accuracy of our positioning estimates against high-precision position data using the RMSE metric. Fig. 7 shows the estimated positions at 10 Hz produced by each method during each blocking period. The blocking durations were 2.5s, 5.0s, 4.0s, 4.0s, 3.0s, and 3.5s (6 periods in total). The high-precision trajectories, sampled at 120 Hz, are shown as green dashed lines.

First, we observed that Gaussian-based methods, such as EKF and iEKF-2, often converged to an incorrect mode

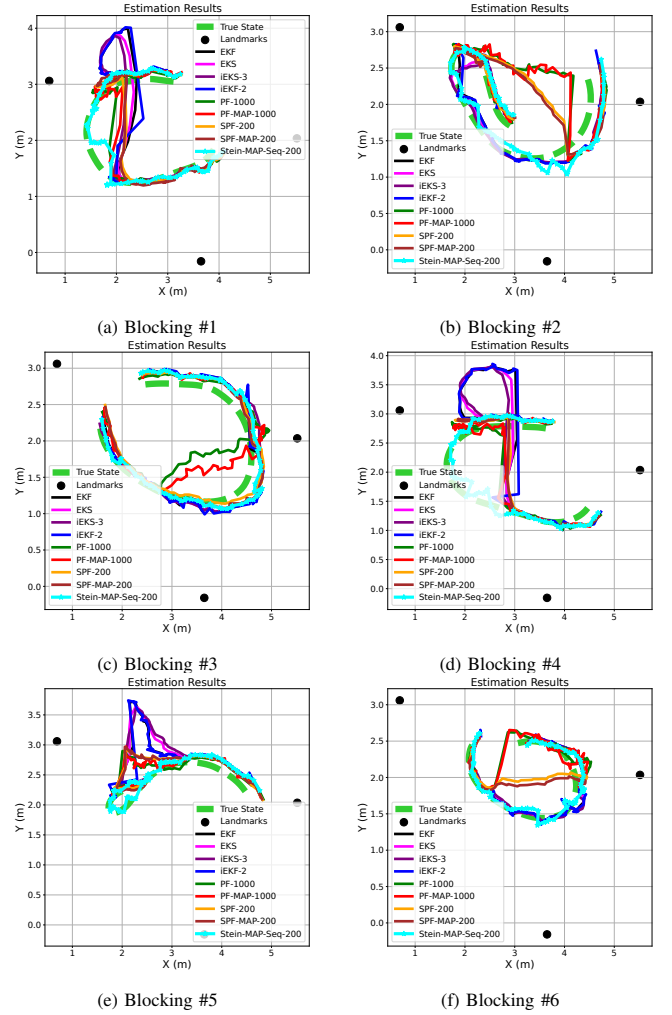


Fig. 7. Estimation results at 10 Hz during each blocking period. Stein-MAP-Seq achieved robust estimation across all multimodal periods.

during most blocking periods. This outcome was examined by analyzing the contour plot of the posterior distribution shown in Fig. 8. To assess the effect of initialization in smoothing or iterative methods, we also implemented EKS-GT and iEKS-3-GT, both initialized with high-precision position data. EKS-GT generally produced estimates close to the high-precision position data due to its locally optimal convergence. In contrast, iEKS-3-GT yielded worse estimates than EKS-GT, with performance degrading further as the number of iterations increased, similar to the position estimation results in Subsection V-B.

In contrast, the PF method can manage non-Gaussian distributions using weighted particles. Nonetheless, it had limitations in fully addressing symmetric multimodality. This is because PF employs the transition model as a proposal distribution for importance sampling, resulting in particle weights that reflect the inherently symmetric, multimodal nature of the likelihood (see Fig. 8). While PF-MAP achieved slightly better performance than PF in handling multimodality—yielding a lower RMSE at certain points—it still could not resolve the symmetric multimodality, resulting in overall performance only marginally better than PF. For PF-MAP-Seq,

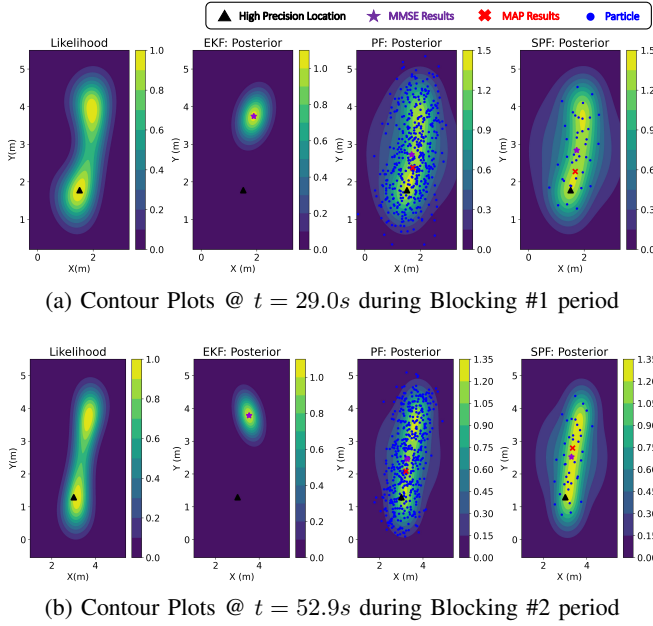


Fig. 8. Contour plots of the Posterior for each method during Blocking #1 and #2 periods.

the symmetric multimodality caused mode switching, which produced worse estimation results than both PF and PF-MAP.

In the case of SPF and SPF-MAP, despite using only 200–400 particles, they outperformed both PF and PF-MAP with 1000–4000 particles in terms of accuracy. However, SPF and SPF-MAP also had limitations in handling symmetric multimodality. As shown in Fig. 8, the particles were positioned according to the gradient flow, allowing a relatively small number of particles to represent the multimodal distribution; however, the symmetric nature of the distribution still led to low estimation accuracy. Table III and Fig. 7 demonstrated that our proposed Stein-MAP-Seq consistently maintains robustness against symmetric multimodal posteriors compared with the other methods.

TABLE III  
ROBUSTNESS EVALUATION FOR SCENARIO (C), RMSE (M)

EKF	EKS	EKS-GT	$N_s$	PF	PF-MAP	PF-MAP-Seq
0.1951	0.1955	<b>0.0886</b>	1e3	0.2014	0.1991	0.4070
			2e3	0.2006	<b>0.1981</b>	0.4217
			4e3	0.2019	0.2003	0.4244
iEKF-2	iEKS-3	iEKS-3-GT	$N_s$	SPF	SPF-MAP	Stein-MAP-Seq
			2e2	0.1933	0.1908	0.1316
			3e2	0.1932	0.1955	<b>0.1273</b>
0.1981	0.1921	0.1243	4e2	0.1931	0.1934	0.1307

## VI. CONCLUSION

State estimation in autonomous systems is a significant challenge, often involving complex scenarios and multimodal distributions in real-world settings. Our estimation methods are designed to handle these multimodal distributions efficiently. In this article, we introduced a MAP sequence estimation method that effectively manages multimodality while reducing computational and memory requirements. The approach is grounded in a sequential variational inference framework that

accounts for dependencies between transition states over time in dynamic system models. Building on this foundation, we addressed MAP sequence estimation through a deterministic gradient flow of particles, embedded within a Viterbi-style dynamic programming framework. To validate our approach, we rigorously evaluated the proposed method in challenging multimodal scenarios, including nonlinear dynamics with ambiguous measurements, pose estimation under unknown data associations, and real-world range-only (wireless) localization under temporary unobservability. Our proposed Stein-MAP-Seq consistently demonstrated robustness across these diverse scenarios.

## APPENDIX

### A. Auxiliary results and proofs

*Lemma A.1:* (Evidence Lower Bound). The relationship between proposal distribution  $q(x_{0:T})$  and  $p(x_{0:T}|z_{1:T})$  can be derived as

$$\text{KL}[q(x_{0:T}) \parallel p(x_{0:T}|z_{1:T})] = -\mathcal{L}(x_{0:T}) + \log p(z_{1:T}), \quad (29)$$

where  $\mathcal{L}(x_{0:T})$  is given in (8).

*Proof:* To address the connection between  $p(x_{0:T}|z_{1:T})$  and  $q(x_{0:T})$ , the representation of  $\log p(x_{0:T}|z_{1:T})$  can be established using the relationship between joint and conditional probabilities given by

$$\log p(x_{0:T}|z_{1:T}) = \log p(x_{0:T}, z_{1:T}) - \log p(z_{1:T}), \quad (30)$$

The proposal distribution  $q(x_{0:T})$  is then introduced by subtracting of  $\log q(x_{0:T})$  from both sides of (30), that is,

$$\log \frac{p(x_{0:T}|z_{1:T})}{q(x_{0:T})} = \log \frac{p(x_{0:T}, z_{1:T})}{q(x_{0:T})} - \log p(z_{1:T}). \quad (31)$$

Note that the expectation of both sides of (31) w.r.t.  $q(x_{0:T})$ ,

$$\begin{aligned} \int q(x_{0:T}) \log \frac{p(x_{0:T}|z_{1:T})}{q(x_{0:T})} dx_{0:T} \\ = \int q(x_{0:T}) \log \frac{p(x_{0:T}, z_{1:T})}{q(x_{0:T})} dx_{0:T} - \log p(z_{1:T}), \end{aligned} \quad (32)$$

where  $\log p(z_{1:T})$  on the right-hand side of (32) is independent of  $x_{0:T}$ . Therefore,  $\int q(x_{0:T}) \log p(z_{1:T}) dx_{0:T} = \log p(z_{1:T})$ . Moreover, the left-hand side of (32) can be expressed using the KL divergence:

$$\begin{aligned} \text{KL}[q(x_{0:T}) \parallel p(x_{0:T}|z_{1:T})] \\ = - \int q(x_{0:T}) \log \frac{p(x_{0:T}, z_{1:T})}{q(x_{0:T})} dx_{0:T} + \log p(z_{1:T}) \geq 0. \end{aligned} \quad (33)$$

□

### B. Proof of Lemma 4.1

The optimal distribution  $q^*(x_{0:T})$  is given as

$$q^*(x_{0:T}) = \underset{q(x_{0:T})}{\operatorname{argmax}} \mathcal{L}(x_{0:T}), \quad (34)$$

where

$$\mathcal{L}(x_{0:T}) = \int q(x_{0:T}) \log p(x_0) dx_{0:T}$$

$$\begin{aligned}
& + \int q(x_{0:T}) \sum_{t=1}^T \log p(x_t|x_{t-1}) dx_{0:T} \\
& + \int q(x_{0:T}) \sum_{t=1}^T \log p(z_t|x_t) dx_{0:T} \\
& - \int q(x_{0:T}) \log q(x_{0:T}) dx_{0:T}. \tag{35}
\end{aligned}$$

The last integral term in (35) can be represented by

$$\begin{aligned}
& - \int q(x_{0:T}) \log q(x_{0:T}) dx_{0:T} = - \int q(x_0) \log q(x_0) dx_0 \\
& - \sum_{t=2}^T \int q(x_{0:T}) \log q(x_t|x_{t-1}, x_{0:t-2}) dx_{0:T}. \tag{36}
\end{aligned}$$

Using the conditional differential entropy [45] as given by

$$- \iint p(x, y) \log p(x|y) dx dy \leq - \int p(x) \log p(x) dx, \tag{37}$$

where equality if and only if  $x$  and  $y$  are independent, we have

$$\begin{aligned}
& - \int q(x_{0:T}) \log q(x_t|x_{t-1}, x_{0:t-2}) dx_{0:T} \\
& \leq - \int q(x_{0:T}) \log q(x_t|x_{t-1}) dx_{0:T}. \tag{38}
\end{aligned}$$

Under Assumption 4.1, there exists

$$q(x_t|x_{t-1}) = q(x_t|x_{t-1}, x_{0:t-2}), \tag{39}$$

and thus  $q(x_{0:T})$  is given via (38) as

$$q(x_{0:T}) = q(x_0) \prod_{t=1}^T q(x_t|x_{t-1}). \tag{40}$$

### C. Proof of Lemma 4.2

Under Lemma 4.1, and considering that  $\log p(x_t|x_{t-1})$  and  $\log p(z_t|x_t)$  depend solely on  $x_t$  and/or  $x_{t-1}$  of  $x_{0:T}$ , the ELBO in (8) is derived from (11):

$$\begin{aligned}
\mathcal{L}(x_{0:T}) &= \int q(x_0) \log p(x_0) dx_0 \\
&+ \sum_{t=1}^T \int q(x_{t:t-1}) \log p(x_t|x_{t-1}) dx_{t:t-1} \\
&+ \sum_{t=1}^T \int q(x_t) \log p(z_t|x_t) dx_t \\
&- \int q(x_{0:T}) \log \left( q(x_0) \prod_{t=1}^T q(x_t|x_{t-1}) \right) dx_{0:T} \\
&= \int q(x_0) \log p(x_0) dx_0 - \int q(x_0) \log q(x_0) dx_0 \\
&+ \sum_{t=1}^T \int q(x_{t:t-1}) \log p(x_t|x_{t-1}) dx_{t:t-1} \\
&+ \sum_{t=1}^T \int q(x_t) \log p(z_t|x_t) dx_t \\
&- \sum_{t=1}^T \int q(x_{t:t-1}) \log q(x_t|x_{t-1}) dx_{t:t-1}. \tag{41}
\end{aligned}$$

Next, we apply the marginalization technique and the law of total probability to demonstrate that the ELBO in (41) can be represented *recursively* as follows:

$$\begin{aligned}
\mathcal{L}(x_{0:T}) &= \int q(x_0) \log p(x_0) dx_0 - \int q(x_0) \log q(x_0) dx_0 \\
&+ \int q(x_1|x_0) q(x_0) \log p(x_1|x_0) dx_{1:0}
\end{aligned}$$

$$\begin{aligned}
&+ \sum_{t=2}^T \int q(x_t|x_{t-1}) q(x_{t-1}|x_{t-2}) \log p(x_t|x_{t-1}) dx_{t:t-1} \\
&+ \int q(x_1|x_0) q(x_0) \log p(z_1|x_1) dx_{1:0} \\
&+ \sum_{t=2}^T \int q(x_t|x_{t-1}) q(x_{t-1}|x_{t-2}) \log p(z_t|x_t) dx_{t:t-2} \\
&- \int q(x_1|x_0) q(x_0) \log q(x_1|x_0) dx_{1:0} \\
&- \sum_{t=2}^T \int q(x_t|x_{t-1}) q(x_{t-1}|x_{t-2}) \log q(x_t|x_{t-1}) dx_{t:t-1}. \tag{42}
\end{aligned}$$

Each term is rearranged based on its dependence on  $x_0$ ,  $x_{1:0}$ , and  $x_{t:t-2}$ , respectively. Then, under Assumption 2.1, the ELBO can be expressed as:

$$\begin{aligned}
\mathcal{L}(x_{0:T}) &= \int q(x_0) \left( \log p(x_0) - \log q(x_0) \right) dx_0 \\
&+ \int \left( \int q(x_1|x_0) \left( \log p(x_1|x_0) + \log p(z_1|x_1) \right. \right. \\
&\quad \left. \left. - \log q(x_1|x_0) \right) dx_1 \right) q(x_0) dx_0 \\
&+ \sum_{t=2}^T \int \left( \int q(x_t|x_{t-1}) \left( \log p(x_t|x_{t-1}) + \log p(z_t|x_t) \right. \right. \\
&\quad \left. \left. - \log q(x_t|x_{t-1}) \right) dx_t \right) q(x_{t-1}|x_{t-2}) dx_{t-1}. \tag{43}
\end{aligned}$$

Therefore, by applying the definition of KL divergence, the ELBO becomes (14).

### D. Proof of Lemma 4.3

We extend the result of [30] to the marginalized conditional KL objective. Define the perturbed distribution as  $q_\epsilon(x_t|x_{t-1}) = \frac{1}{N_s} \sum_{i=1}^{N_s} \delta(x_t - (x_t^i + \epsilon \hat{\phi}^*(x_t^i)))$ , where the perturbation follows the update in (17). Under Assumption 4.1, Lemma 4.1, and 4.2, the corresponding marginalized KL divergence objective becomes

$$\mathcal{J}_t(q_\epsilon) = \int \text{KL}[q_\epsilon(x_t|x_{t-1}) \| p(z_t, x_t|x_{t-1})] q(x_{t-1}|x_{t-2}) dx_{t-1}.$$

We compute its directional derivative at  $\epsilon = 0$  as follows

$$\begin{aligned}
& \frac{d}{d\epsilon} \mathcal{J}_t(q_\epsilon) \Big|_{\epsilon=0} \\
&= \int \frac{d}{d\epsilon} \text{KL}[q_\epsilon(x_t|x_{t-1}) \| p(z_t, x_t|x_{t-1})] \Big|_{\epsilon=0} q(x_{t-1}|x_{t-2}) dx_{t-1}. \tag{44}
\end{aligned}$$

Using Stein variational theory, the directional derivative of the KL divergence for fixed  $x_{t-1}$  is

$$\begin{aligned}
& \frac{d}{d\epsilon} \text{KL}[q_\epsilon(x_t|x_{t-1}) \| p(z_t, x_t|x_{t-1})] \Big|_{\epsilon=0} \\
&= -\mathbb{E}_{q(x_t|x_{t-1})} \left[ \phi(x_t)^\top \nabla_{x_t} \log p(z_t, x_t|x_{t-1}) + \nabla \cdot \phi(x_t) \right], \tag{45}
\end{aligned}$$

where  $\nabla \cdot \phi(x_t)$  is the divergence of  $\phi(x_t)$ . Then, substituting (45) into the expression for  $\mathcal{J}_t(q_\epsilon)$  in (44), we obtain

$$\begin{aligned}
& \frac{d}{d\epsilon} \mathcal{J}_t(q_\epsilon) \Big|_{\epsilon=0} \\
&= -\int \mathbb{E}_{q(x_t|x_{t-1})} \left[ \phi(x_t)^\top \nabla_{x_t} \log p(z_t, x_t|x_{t-1}) + \nabla \cdot \phi(x_t) \right] \\
&\quad \times q(x_{t-1}|x_{t-2}) dx_{t-1}. \tag{46}
\end{aligned}$$



Using the Stein operator  $\mathcal{A}_p\phi(x_t)$ , the derivative becomes

$$\left. \frac{d}{d\epsilon} \mathcal{J}_t(q_\epsilon) \right|_{\epsilon=0} = -\mathbb{E}_{q(x_{t-1}|x_{t-2})} \left[ \mathbb{E}_{q(x_t|x_{t-1})} [\text{tr}(\mathcal{A}_p\phi(x_t))] \right]. \quad (47)$$

where  $\mathcal{A}_p\phi(x_t) := \nabla_{x_t} \log p(z_t, x_t|x_{t-1})\phi(x_t)^\top + \nabla_{x_t}\phi(x_t)$  and  $\text{tr}(\cdot)$  denotes the trace operator. Under Assumption 2.1 and the assumption of the boundedness of the kernel  $\kappa(\cdot, \cdot)$ , the SVGD direction  $\phi^* \in \mathcal{H}^d$  is chosen to maximize the negative directional derivative. Therefore,

$$\left. \frac{d}{d\epsilon} \mathcal{J}_t(q_\epsilon) \right|_{\epsilon=0} < 0, \quad (48)$$

unless  $q(x_t|x_{t-1}) = p(z_t, x_t|x_{t-1})$  almost surely under  $q(x_{t-1}|x_{t-2})$ .

### E. Proof of Theorem 4.1

First, we prove that the ELBO in (14) converges to  $J(s)$  as  $\epsilon \rightarrow 0$  by using a standard property of mollifiers [46]. From (14) in Lemma 4.2, we have

$$\begin{aligned} \mathcal{L}_\epsilon(q_\epsilon) &= \mathbb{E}_{q_\epsilon(x_0)} [\log p(x_0)] + \mathbb{E}_{q_\epsilon(x_0)} \mathbb{E}_{q_\epsilon(x_1|x_0)} [\log p(z_1, x_1|x_0)] \\ &+ \sum_{t=2}^T \mathbb{E}_{q_\epsilon(x_{t-1}|x_{t-2})} \mathbb{E}_{q_\epsilon(x_t|x_{t-1})} [\log p(z_t, x_t|x_{t-1})]. \end{aligned} \quad (49)$$

By Assumption 2.1 and using a Gaussian as a mollifier (approximate identity) [47],  $\mathbb{E}_{q_\epsilon(\cdot)} [\log p] \rightarrow \log p(s)$  as  $\epsilon \rightarrow 0$ . Applying this to each term above yields

$$\begin{aligned} \lim_{\epsilon \rightarrow 0} \mathcal{L}_\epsilon(q_\epsilon) &= \log p(s_0) + \log p(z_1, s_1|s_0) + \sum_{t=2}^T \log p(z_t, s_t|s_{t-1}) \\ &= J(s) \end{aligned} \quad (50)$$

Second, we prove that  $\mathcal{L}_\epsilon(s^*)$  is the maximizer over  $\mathcal{S}$ . Since  $\mathcal{S}$  is finite and there exists a unique  $s^* \in \arg \max_{s \in \mathcal{S}} J(s)$  with gap  $\delta = J(s^*) - \max_{s \neq s^*} J(s) > 0$ , it follows from (50) that

$$M_\epsilon := \max_{s \in \mathcal{S}} |\mathcal{L}_\epsilon(s) - J(s)| \xrightarrow{\epsilon \rightarrow 0} 0. \quad (51)$$

Choose  $\epsilon_0 > 0$  such that  $M_\epsilon < \delta/3$  for all  $0 < \epsilon < \epsilon_0$ . Then, for such  $\epsilon$ ,

$$\begin{aligned} \mathcal{L}_\epsilon(s^*) &\geq J(s^*) - \frac{\delta}{3}, \\ \mathcal{L}_\epsilon(s) &\leq J(s) + \frac{\delta}{3} \leq J(s^*) - \delta + \frac{\delta}{3} = J(s^*) - \frac{2\delta}{3}, \quad \forall s \neq s^*. \end{aligned}$$

Therefore,  $\mathcal{L}_\epsilon(s^*) > \mathcal{L}_\epsilon(s), \forall s \neq s^*$ , hence, the maximizer of  $\mathcal{L}_\epsilon$  over  $\mathcal{S}$  coincides with  $s^*$ .

### REFERENCES

- [1] Y. Li, C. Lee, and V. Monga, "A maximum a posteriori estimation framework for robust high dynamic range video synthesis," *IEEE Transactions on Image Processing*, vol. 26, no. 3, pp. 1143–1157, 2016.
- [2] N. Kanda, X. Lu, and H. Kawai, "Maximum-a-posteriori-based decoding for end-to-end acoustic models," *IEEE/ACM Transactions on Audio, Speech, and Language Processing*, vol. 25, no. 5, pp. 1023–1034, 2017.
- [3] A. Abdolmaleki, J. T. Springenberg, Y. Tassa, R. Munos, N. Heess, and M. Riedmiller, "Maximum a posteriori policy optimisation," *arXiv preprint arXiv:1806.06920*, 2018.
- [4] M. Z. Islam, C.-M. Oh, J. S. Lee, and C.-W. Lee, "Multi-part histogram based visual tracking with maximum of posteriori," in *2010 2nd International Conference on Computer Engineering and Technology*, vol. 6, pp. V6–435, IEEE, 2010.
- [5] G. Huang, K. Zhou, N. Trawny, and S. I. Roumeliotis, "A bank of maximum a posteriori (map) estimators for target tracking," *IEEE Transactions on Robotics*, vol. 31, no. 1, pp. 85–103, 2015.
- [6] F. Dellaert, M. Kaess, et al., "Factor graphs for robot perception," *Foundations and Trends® in Robotics*, vol. 6, no. 1-2, pp. 1–139, 2017.
- [7] M. Svensén and C. M. Bishop, "Pattern recognition and machine learning," 2007.
- [8] J. Trogh, D. Plets, L. Martens, and W. Joseph, "Advanced indoor localisation based on the Viterbi algorithm and semantic data," in *2015 9th European Conference on Antennas and Propagation (EuCAP)*, pp. 1–3, IEEE, 2015.
- [9] M. Scherhäufl, B. Rudić, A. Stelzer, and M. Pichler-Scheder, "A blind calibration method for phase-of-arrival-based localization of passive UHF RFID transponders," *IEEE Transactions on Instrumentation and Measurement*, vol. 68, no. 1, pp. 261–268, 2018.
- [10] S. Sun, Y. Li, W. S. Rowe, X. Wang, A. Kealy, and B. Moran, "Practical evaluation of a crowdsourcing indoor localization system using hidden Markov models," *IEEE Sensors Journal*, vol. 19, no. 20, pp. 9332–9340, 2019.
- [11] A. Bayoumi, P. Karkowski, and M. Bennewitz, "Speeding up person finding using hidden Markov models," *Robotics and Autonomous Systems*, vol. 115, pp. 40–48, 2019.
- [12] M.-W. Seo and S. S. Kia, "Online target localization using adaptive belief propagation in the HMM framework," *IEEE Robotics and Automation Letters*, vol. 7, no. 4, pp. 10288–10295, 2022.
- [13] M.-W. Seo and S. S. Kia, "Bayesian online learning for human-assisted target localization," *Automatica*, vol. 177, p. 112288, 2025.
- [14] C. Champlin and D. Morrell, "Target tracking using irregularly spaced detectors and a continuous-state Viterbi algorithm," in *Conference Record of the Thirty-Fourth Asilomar Conference on Signals, Systems and Computers (Cat. No. 00CH37154)*, vol. 2, pp. 1100–1104, IEEE, 2000.
- [15] P. Chigansky and Y. Ritov, "On the Viterbi process with continuous state space," *Bernoulli*, vol. 17, no. 2, pp. 609–627, 2011.
- [16] S. Godsill, A. Doucet, and M. West, "Maximum a posteriori sequence estimation using Monte Carlo particle filters," *Annals of the Institute of Statistical Mathematics*, vol. 53, pp. 82–96, 2001.
- [17] J. Driessen, "Particle filter MAP estimation in dynamical systems," in *The IET Seminar on Target Tracking and Data Fusion Algorithms and Applications, Birmingham, UK, 2008*, pp. 1–25, 2008.
- [18] S. Saha, Y. Boers, H. Driessen, P. K. Mandal, and A. Bagchi, "Particle based MAP state estimation: A comparison," in *2009 12th International Conference on Information Fusion*, pp. 278–283, IEEE, 2009.
- [19] T. Nishida, W. Kogushi, N. Takagi, and S. Kurogi, "Dynamic state estimation using particle filter and adaptive vector quantizer," in *2009 IEEE International Symposium on Computational Intelligence in Robotics and Automation-(CIRA)*, pp. 429–434, IEEE, 2009.
- [20] M. Morita and T. Nishida, "Fast Maximum A Posteriori Estimation using Particle Filter and Adaptive Vector Quantization," in *2020 59th Annual Conference of the Society of Instrument and Control Engineers of Japan (SICE)*, pp. 977–982, IEEE, 2020.
- [21] D. M. Blei, A. Kucukelbir, and J. D. McAuliffe, "Variational inference: A review for statisticians," *Journal of the American Statistical Association*, vol. 112, no. 518, pp. 859–877, 2017.
- [22] J. Ala-Luhtala, R. Piché, and S. Särkkä, "Variational inference for state-space models with point process observations," in *2013 IEEE International Conference on Acoustics, Speech and Signal Processing*, pp. 6302–6306, IEEE, 2013.
- [23] Y. Gal, "Uncertainty in deep learning," *University of Cambridge*, vol. 1, no. 3, 2016.
- [24] E. Archer, I. M. Park, L. Buesing, J. Cunningham, and L. Paninski, "Black box variational inference for state space models," in *International Conference on Learning Representations*, 2015.
- [25] R. G. Krishnan, U. Shalit, and D. Sontag, "Structured inference networks for nonlinear state space models," *Proceedings of the AAAI Conference on Artificial Intelligence*, vol. 31, no. 1, 2017.
- [26] M.-W. Seo and S. S. Kia, "Sequential gaussian variational inference for nonlinear state estimation and its application in robot navigation," *IEEE Robotics and Automation Letters*, 2024.
- [27] A. Mirchev, B. Kayalibay, P. van der Smagt, and J. Bayer, "Variational state-space models for localisation and dense 3d mapping in 6 dof," *International Conference on Learning Representations (ICLR)*, 2021.

- [28] T. D. Barfoot, J. R. Forbes, and D. J. Yoon, “Exactly sparse Gaussian variational inference with application to derivative-free batch nonlinear state estimation,” *The International Journal of Robotics Research*, vol. 39, no. 13, pp. 1473–1502, 2020.
- [29] S. Oh, “Variational bayesian multiobject tracking using robust appearance model,” *IEEE Transactions on Signal Processing*, vol. 68, pp. 5749–5763, 2020.
- [30] Q. Liu and D. Wang, “Stein variational gradient descent: A general purpose bayesian inference algorithm,” *Advances in neural information processing systems*, vol. 29, 2016.
- [31] L. Barcelos, A. Lambert, R. Oliveira, P. Borges, B. Boots, and F. Ramos, “Dual online Stein variational inference for control and dynamics,” *Robotics: Science of Systems (RSS)*, 2021.
- [32] Z. Wang, O. So, J. Gibson, B. Vlahov, M. S. Gandhi, G.-H. Liu, and E. A. Theodorou, “Variational inference mpc using tsallis divergence,” *Robotics: Science of Systems (RSS)*, 2021.
- [33] F. A. Maken, F. Ramos, and L. Ott, “Stein ICP for uncertainty estimation in point cloud matching,” *IEEE Robotics and Automation Letters*, vol. 7, no. 2, pp. 1063–1070, 2021.
- [34] F. A. Maken, F. Ramos, and L. Ott, “Stein particle filter for nonlinear, non-Gaussian state estimation,” *IEEE Robotics and Automation Letters*, vol. 7, no. 2, pp. 5421–5428, 2022.
- [35] E. Heiden, C. E. Denniston, D. Millard, F. Ramos, and G. S. Sukhatme, “Probabilistic inference of simulation parameters via parallel differentiable simulation,” in *2022 International Conference on Robotics and Automation (ICRA)*, pp. 3638–3645, IEEE, 2022.
- [36] S. Kullback and R. A. Leibler, “On information and sufficiency,” *The annals of mathematical statistics*, vol. 22, no. 1, pp. 79–86, 1951.
- [37] J. Courts, A. G. Wills, T. B. Schön, and B. Ninness, “Variational system identification for nonlinear state-space models,” *Automatica*, vol. 147, p. 110687, 2023.
- [38] F. Gustafsson, “Particle filter theory and practice with positioning applications,” *IEEE Aerospace and Electronic Systems Magazine*, vol. 25, no. 7, pp. 53–82, 2010.
- [39] A. Gelb *et al.*, *Applied optimal estimation*. MIT press, 1974.
- [40] A. Doucet, N. De Freitas, and N. Gordon, “An introduction to sequential Monte Carlo methods,” *Sequential Monte Carlo methods in practice*, pp. 3–14, 2001.
- [41] S. Särkkä and L. Svensson, *Bayesian filtering and smoothing*, vol. 17. Cambridge university press, 2023.
- [42] Á. F. García-Fernández, L. Svensson, and S. Särkkä, “Iterated posterior linearization smoother,” *IEEE Transactions on Automatic Control*, vol. 62, no. 4, pp. 2056–2063, 2016.
- [43] E. Olson, J. J. Leonard, and S. Teller, “Robust range-only beacon localization,” *IEEE Journal of Oceanic Engineering*, vol. 31, no. 4, pp. 949–958, 2006.
- [44] C. Chen and S. S. Kia, “Cooperative localization using learning-based constrained optimization,” *IEEE Robotics and Automation Letters*, vol. 7, no. 3, pp. 7052–7058, 2022.
- [45] R. B. Ash, *Information theory*. Courier Corporation, 2012.
- [46] H. Brezis and H. Brézis, *Functional analysis, Sobolev spaces and partial differential equations*, vol. 2. Springer, 2011.
- [47] E. M. Stein and R. Shakarchi, “Fourier analysis. an introduction. princeton lectures in analysis, 1,” *Princeton, NJ: Princeton Univ. Press. MR1970295*, vol. 44, p. 45, 2003.